

# Hidden Markov Model for Multidimensional Wavefront Tracking

Monica Nicoli, *Member, IEEE*, Vittorio Rampa, and Umberto Spagnolini, *Member, IEEE*

**Abstract**—In subsurface sensing, the estimation of the delays (wavefronts) of the backscattered wavefields is a very time-consuming, mostly manual task. We propose delay estimation by exploiting the continuity of the wavefronts modeled as a Markov chain. Each wavefront is a realization of Brownian motion with a correlation that depends on the distance between each source/receiver pair. Therefore, the delay profiles can be tracked with any known method by assuming that the *ordered* sequence of signals is described by a hidden Markov model (HMM).

Linear array provides the most natural data-ordering, and in this case the tracking algorithms can preserve the target/tracker association. However, when measurements are multidimensional, the volume-slicing strategies, that are able to get a linear array of (virtually) ordered signals, select the measurements independently of the target. When different estimates along slices are merged mis-ties can occur easily. Since data-ordering is a main issue for irregularly positioned sources and receivers, we propose a region growing tracking technique that orders (for each specified target) the data while tracking. The ordering is based on the maximum *a posteriori* probability of detection. Experiments based on multidimensional measurements show that this region growing tracking algorithm based on HMM preserves the target/tracker association.

**Index Terms**—Array processing, delay estimation, detection and estimation, geophysics, hidden Markov model (HMM), horizon picking, irregular sampling, multidimensional signal processing, region growing algorithm, target tracking, Viterbi algorithm.

## I. INTRODUCTION

**I**N SUBSURFACE sensing, the characteristics of the propagating medium are investigated by creating perturbations with a source (or an array of sources) and measuring with a receiver (or an array of receivers) the wavefield backscattered by points and/or three-dimensional (3-D) surfaces (or reflectors). In order to improve the resolution, wideband pulse-like signals are usually employed.

In oil exploration, wavefront tracking (also referred as horizon picking [1]) is carried out during the interpretation stage. Any *a priori* knowledge of the structure and the stratigraphy of the investigated area is of great help in the manual interpretation of seismic sections. Algorithms based on probabilistic data association [2] and neural networks [3] have been proposed to aid manual tracking. Markov random fields have been proposed in deconvolution to add spatial continuity in

reflectivity [4]. It is only recently that the multidimensionality of the dataset has been exploited by integrating the differential delays estimated for all the neighboring sensor pairs [5]. This method estimates the wavefront globally, with minimum interaction during the manual interpretation step (except for target pre-windowing). However, the aforementioned method is based on the implicit assumption that the wavefront is a single-valued continuous function. In some cases, as for the faulty areas, this can be a severe drawback that is removed here by assuming a statistical model for discontinuous wavefront.

The multidimensional wavefront tracking problem can be stated as follows. Let  $\{d(\mathbf{x}_i, t)\}_{i=1}^N$  be a set of  $N$  measurements, where  $d(\mathbf{x}_i, t)$  is related to the source–receiver pair ( $i = 1, \dots, N$ ) that is uniquely identified by the  $n$ -dimensional set  $\mathbf{x}_i$  of spatial coordinates ( $n \leq 6$  as there are up to three spatial coordinates for sources  $(x_s, y_s, z_s)$  and receivers  $(x_r, y_r, z_r)$ ). The purpose is to estimate the delay function  $\tau^{(\ell)}(\mathbf{x}_i)$  of the wavefront backscattered by the  $\ell$ th reflector from the knowledge of the signature and the statistical properties of the wavefront modeled as a correlated random process. The backscattering surfaces are assumed to have fractal properties [6] where the correlation of the delays across the wavefront depends on the distance between each source/receiver pair. The delay can be quantized in a set of disjointed states and the wavefront evolves as a Markov chain. The ordered sequence of signals is thus described by an HMM. According to this statistical model, it is straightforward to estimate  $\tau^{(\ell)}(\mathbf{x}_i)$  from the whole dataset by extending the state-sequence tracking methods based on the HMM such as the backward/forward, Viterbi and detection/tracking algorithm [7]. HMM algorithms have been considered recently by the remote sensing community as a powerful processing tool for the integration of multiple measurements. For instance, the classification of unexploded ordinance [8] can be based on its shape [9]. Extension from frequency-line tracking in [10] and [11] to the tracking of delays of wideband echoes has been investigated recently for  $\{d(x_i, t)\}$ , with  $n = 1$  spatial dimensions [7], as a generalization of the detection/tracking algorithm proposed in [12].

The multidimensionality of the wavefront arises from the complex arrangements of the  $N$  source/receiver pairs in space. For instance, when the source location is fixed, and receivers are placed throughout in the space, we have a common source experiment:  $\mathbf{x} = (x_r, y_r, z_r)$  and  $n \leq 3$ . On the contrary, the common receiver experiment is made by moving the sources around:  $\mathbf{x} = (x_s, y_s, z_s)$  and  $n \leq 3$ . Cross-spreads are obtained when sources and receivers move along two orthogonal lines as depicted in Fig. 1 ( $n = 2$ ). In any case, the set  $\{d(\mathbf{x}_i, t)\}_{i=1}^N$  is

Manuscript received April 5, 2001; revised September 4, 2001.

M. Nicoli and U. Spagnolini are with the Dipartimento di Elettronica e Informazione, Politecnico di Milano, I-20133 Milano, Italy (e-mail: nicoli@elet.polimi.it, spagnoli@elet.polimi.it).

V. Rampa is with the CSTS-CNR, Politecnico di Milano, I-20133 Milano, Italy (e-mail: rampa@elet.polimi.it).

Publisher Item Identifier S 0196-2892(02)03266-7.

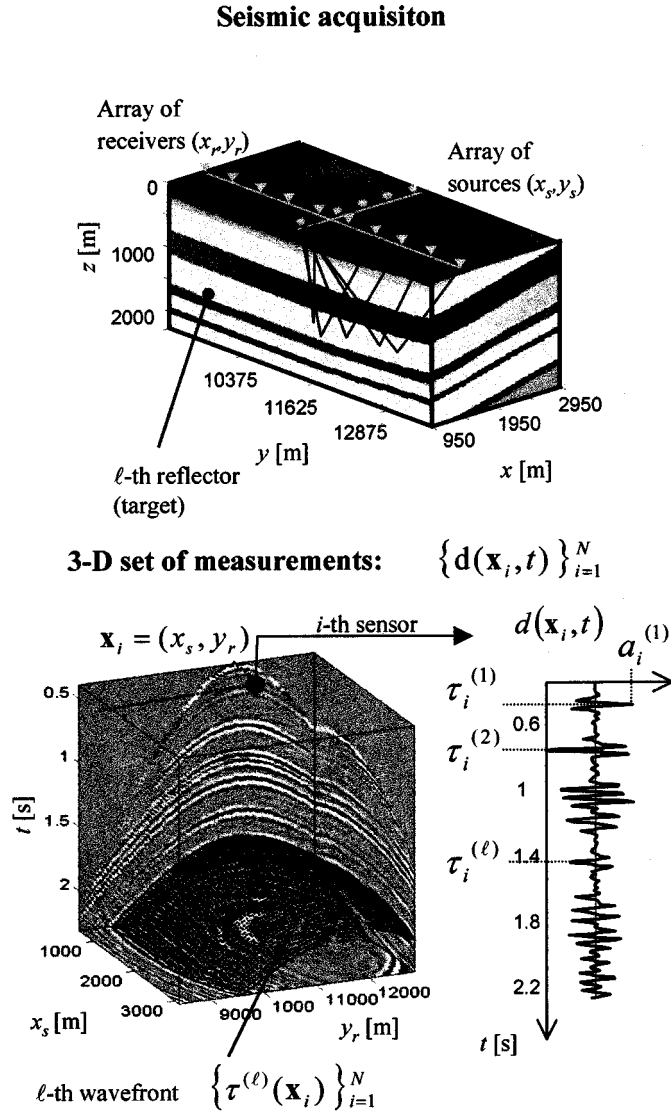


Fig. 1. Example of seismic acquisition with sources and receivers along two crossing lines (cross-spread acquisition). Each measurement  $d(\mathbf{x}_i, t)$  is identified by the  $n = 2$  spatial coordinates  $\mathbf{x}_i$  for the  $i$ th source/receiver pair. The data volume is 3-D. From top to bottom: propagating medium (top), data volume sliced along two axes with the  $\ell$ th backscattered wavefront  $\tau^{(\ell)}(\mathbf{x})$  superimposed (bottom left), detailed view of the signal  $d(\mathbf{x}_i, t)$  in  $\mathbf{x}_i$  (bottom right).

a volume of  $n + 1$  dimensions (see the 3-D volume in Fig. 1). Similar to [5], it is convenient to consider each measurement  $d(\mathbf{x}_i, t)$  as being virtually obtained by a sensor placed at location  $\mathbf{x}_i$ . Later in this paper,  $\mathbf{x}_i$  will be referred to as the sensor position. According to this arrangement, the delay function  $\tau^{(\ell)}(\mathbf{x}_i)$  is characterized by the *hyper-surface* in the  $(n + 1)$ -dimensional space (see also Fig. 1 for the case  $\mathbf{x} = (x_s, y_r)$  and  $n = 2$ ). Remember that the wavefront is always associated with a specific backscattering reflector that is the true target in the experiment. The association can be easily determined when the propagating medium is simple (or stratified as in Fig. 1) but it becomes less evident when the medium is more complex. For instance, crossing wavefronts can be the result of diffractions from the same target and, in this case, numerical back-propagation of the backscattered wavefield (or migration

[13]) is needed before attempting any association between the crossing wavefronts and the target. The estimation of delay profiles of backscattered wavefields and their association with the corresponding targets are time-consuming tasks that are carried out manually by heuristically exploiting the correlation properties of the wavefront. The target/tracker association is even more difficult when the source/receiver pairs are irregularly positioned and/or their layout is sparse.

Extension of HMM for delay tracking for  $n = 1$  [7] to nonuniformly spaced source/receiver positions with  $n > 1$  is mostly limited by the need to order the observations into a sequence of data so that the Markov model describing the state transitions contains informative *a priori* probabilities. Data-ordering strategy should be designed so as to preserve the target/tracker association, even when the wavefronts are not isolated. To perform the data-ordering, sensor selection cannot be carried out disjointedly from the target, as this does not guarantee keeping the target/tracker association. Here we propose to order the data *while* tracking, by selecting those measurements that maximize the *a posteriori* probability of detection. The selection is based on a region growing method that let a subset of data  $\{d(\mathbf{x}_i, t)\}_{i=1}^k$  grow to include (and track) a new data  $d(\mathbf{x}_{k+1}, t)$  chosen from the neighborhood of the subset  $\{\mathbf{x}_i\}_{i=1}^k$  already tracked. Multitarget is performed iteratively as in [12] with a considerable reduction of the computational complexity with respect to true multitarget algorithms.

The paper is organized as follows: the problem definition and the statistical model are described in Section II; HMM and the tracking algorithms are shown in Section III for  $n = 1$  and in Section IV for  $n \geq 2$  (region growing tracking). In Section V the advantages of the multidimensional tracking are compared with the slicing algorithm.

## II. PROBLEM STATEMENT

The backscattered wavefield measured by the  $i$ th sensor ( $i = 1, \dots, N$ ) at space location  $\mathbf{x}_i$  is modeled as a combination of  $L_i$  echoes with known signature  $w(t)$

$$d(\mathbf{x}_i, t) = \sum_{\ell=1}^{L_i} c_i^{(\ell)} w(t - \tau_i^{(\ell)}) + n(\mathbf{x}_i, t). \quad (1)$$

For the echo associated with the  $\ell$ th target,  $c_i^{(\ell)}$  denotes the amplitude and  $\tau_i^{(\ell)} = \tau^{(\ell)}(\mathbf{x}_i)$  is the delay. For backscattered signals  $c_i^{(\ell)}$  is scaled to the transmitted signature so that  $|c_i^{(\ell)}| \leq 1$ .  $n(\mathbf{x}_i, t)$  is the zero mean spatially and temporally uncorrelated Gaussian noise with variance  $\sigma_n^2$ , the signal to noise ratio (SNR) is  $\rho = E_w / \sigma_n^2$  where  $E_w$  is the energy of the source signature. The number of echoes  $L_i$  can change from one sensor to the neighboring one according to the number of targets and it is assumed to be bounded:  $0 \leq L_i \leq L$ . The time-sampled signal  $d(\mathbf{x}_i, t_k) = d(\mathbf{x}_i, k \cdot \Delta t)$  is arranged in a column vector  $\mathbf{d}_i = [d(\mathbf{x}_i, t_1), \dots, d(\mathbf{x}_i, t_M)]^T$ . The discrete-time model (1) reduces to

$$\mathbf{d}_i = \sum_{\ell=1}^{L_i} c_i^{(\ell)} \mathbf{w}(\tau_i^{(\ell)}) + \mathbf{n}_i \quad (2)$$

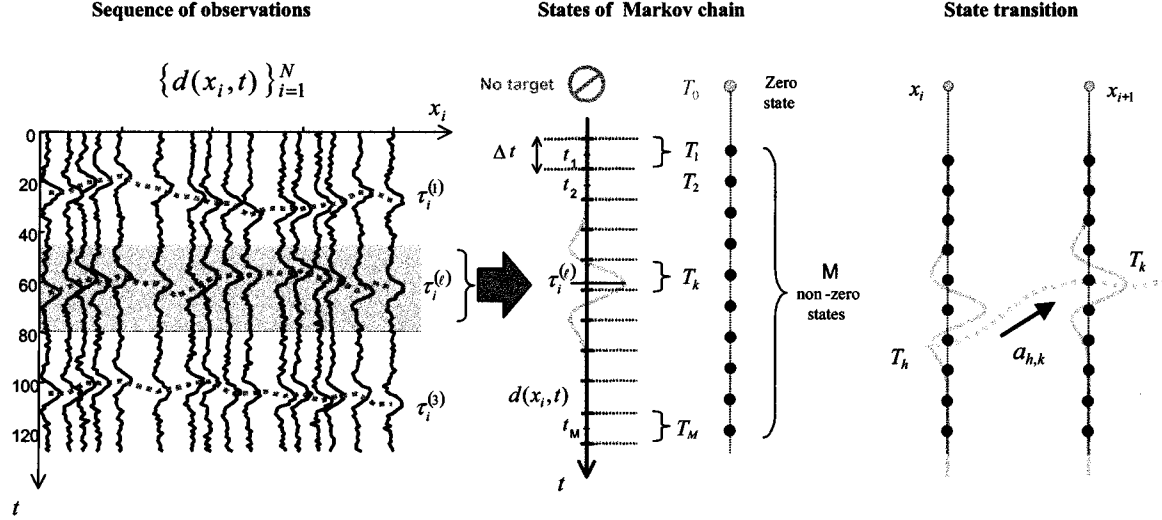


Fig. 2. HMM for delay tracking. From left to right: example of a set of unevenly spaced observations  $\{d(\mathbf{x}_i, t)\}_{i=1}^N$  for  $n = 1$ , each target (shaded area) is modeled as Markov chain (left); delayed signature and states of the Markov chain for the  $\ell$ th delay function including the zero-state (center); probabilities of state transition (right).

where  $\mathbf{w}(\tau_i^{(\ell)}) = [w(t_1 - \tau_i^{(\ell)}), \dots, w(t_M - \tau_i^{(\ell)})]^T$  are the  $M$  samples for the signature delayed by  $\tau_i^{(\ell)}$  and  $\mathbf{n}_i = [n(\mathbf{x}_i, t_1), \dots, n(\mathbf{x}_i, t_M)]^T$ . The wavefront tracking problem can be stated as follows: given the set of *ordered* sequence of observations  $\mathbf{D}_N = [\mathbf{d}_1, \dots, \mathbf{d}_N]$  (see e.g., Fig. 2) estimate the sequence of delays  $\{\tau_i^{(\ell)}\}_{i=1}^N$  for the  $\ell$ th target ( $\ell = 1, \dots, L$ ). This can be done 1) by preserving the association between delays and target and 2) by exploiting the *a priori* information about the target continuity.

The wavefront  $\tau_i^{(\ell)}$  can be modeled as a random process where the increment  $\tau_{i+1}^{(\ell)} - \tau_i^{(\ell)}$  is Gaussian with variance

$$\sigma_{i+1,i}^2 = E \left[ \left( \tau_{i+1}^{(\ell)} - \tau_i^{(\ell)} \right)^2 \right] = \chi^{(\ell)} \|\mathbf{x}_{i+1} - \mathbf{x}_i\| \quad (3)$$

that depends linearly on the distance between the two sensors while the scaling factor  $\chi^{(\ell)}$  depends on the target. For uniform wavefront sampling, the term  $\sigma_{i+1,i}^2$  is constant:  $\sigma_{i+1,i}^2 = \sigma^2$ . The delay function can be modeled as a generalized random walk  $\tau_{i+1}^{(\ell)} = \tau_i^{(\ell)} + v_i^{(\ell)}$ , where  $v_i^{(\ell)} \sim \mathcal{N}(0, \sigma^2)$  is the driving process. When sensor positioning is irregular, the driving process is  $v_i^{(\ell)} \sim \mathcal{N}(0, \sigma_{i+1,i}^2)$ . Since  $\sigma_{i+1,i}^2$  increases linearly with distance (3), the delay sequence associated with the same target is more reliably estimated when the distance  $\|\mathbf{x}_{i+1} - \mathbf{x}_i\|$  is small, as the *a priori* information on target continuity, or its smoothness, is informative for the delay tracking (see Section III). This is the basis of commonly agreed on heuristic criteria that relate the delays for neighboring sensors.

Quality of delay tracking depends on data ordering. There is no *a priori* criteria to select the observations; data ordering is even more difficult when dealing with complex source/receiver arrangements as in the  $n$ -D set  $\mathbf{x}$  ( $n \leq 6$ ). According to the model (3), an ordering of the observations based on the neighboring selection criteria is preferable as the delay/target association can be preserved mostly by extrapolating the features of the targets already tracked. The continuity property of the delays

depends on the continuity of the targets modeled in Section III as first order Markov chain. Even if this statistical model describes appropriately the delays for ordered and evenly spaced observations (i.e., for  $n = 1$ ), we now extend the model to any source/receiver arrangements by ordering the observations  $[\mathbf{d}_1, \dots, \mathbf{d}_N]$  while tracking, still based on a neighboring selection criterion. This is the key point in the extension of the delay tracking discussed below for  $n = 1$  (Section III) and  $n \geq 2$  array (Section IV).

### III. HMM FOR DELAY TRACKING ( $n = 1$ )

For one target ( $L_i \leq L = 1$ ) and  $n = 1$  the model (2) reduces to a sequence of ordered observations

$$\mathbf{d}_i = c_i \mathbf{w}(\tau_i) + \mathbf{n}_i \quad (4)$$

where indexes not strictly necessary are dropped (even if  $L > 1$ , the reasoning can be reduced to the case  $L = 1$  by windowing the observations as sketched in Fig. 2). Tracking methods are based on modeling the delays [14]. Here  $\tau_i$  is modeled as a generalized random walk where the variance  $\sigma_{i+1,i}^2$  depends on the spacing of the pair of sensors. The set  $\{d(\mathbf{x}_i, t)\}_{i=1}^N$  is a first order HMM (shaded area in Fig. 2) and is thus characterized by an underlying (hidden) Markov chain having a finite number of states and a set of random functions generating the observations. The complete specification of the HMM requires the definition of the set of states and the probabilities for the state transitions, the observations and the initial state.

#### A. Hidden Markov Model

Let the set of  $M + 1$  states be  $\mathbf{T} = \{T_0, T_1, \dots, T_M\}$ , each nonzero state  $T_k$  (for  $k \neq 0$ ) is associated with the  $k$ th time interval as shown in Fig. 2.  $\tau_i = T_k$  denotes that the generic delay  $\tau_i \in [t_k - \Delta t/2, t_k + \Delta t/2)$  is quantized and is assigned to  $T_k$  regardless of its actual location within the time interval. The union of the nonzero states is associated with the existence of the backscattered echo at the  $i$ th position: this is named hypothesis

$H_1(\mathbf{x}_i)$  where  $H_1(\mathbf{x}_i) = \{\tau_i \in \bigcup_{k=1}^M T_k\}$ , note that,  $\forall k \neq h$ , it is  $T_k \cap T_h = \emptyset$ . The zero state  $T_0$  is included to allow target initiation and termination; therefore  $\tau_i = T_0$  indicates that there is no target at the  $i$ th position. The null hypothesis is defined as  $H_0(\mathbf{x}_i) = \{\tau_i = T_0\}$ .

The delay function is described by the sequence of states according to the transition probabilities  $a_{h,k}$  between each couple of states  $h$  and  $k$ :  $a_{h,k} = p[\tau_{i+1} = T_k | \tau_i = T_h]$ . The transition probabilities involving the zero state  $\vartheta = p[\tau_{i+1} \neq T_0 | \tau_i = T_0]$  and  $\nu = p[\tau_{i+1} = T_0 | \tau_i \neq T_0]$  denote the probability of target initiation and termination, respectively. By assuming that the target initiation and termination are independent of the nonzero state  $T_k$ , it follows that

$$\begin{aligned} a_{0,0} &= 1 - \vartheta \\ a_{0,k} &= \frac{\vartheta}{M}, \quad k \neq 0 \\ a_{h,0} &= \nu, \quad h \neq 0. \end{aligned} \quad (5)$$

For the nonzero states the probability of transition from the  $h$ th cell to the  $k$ th cell is computed using  $g_{h,k} = p[\tau_{i+1} = T_k | \tau_i = T_h]$ ,  $\forall h, k = 1, \dots, M$ , that can be calculated according to the Gaussian assumption for the driving process

$$\begin{aligned} g_{h,k} &= \int_{t_k - (\Delta t/2)}^{t_k + (\Delta t/2)} \frac{1}{\sqrt{2\pi}\sigma_{i+1,i}} \exp\left(-\frac{(\tau - t_h)^2}{2\sigma_{i+1,i}^2}\right) d\tau \\ &\simeq \frac{\Delta t}{\sqrt{2\pi}\sigma_{i+1,i}} \exp\left(-\frac{\Delta t^2(k-h)^2}{2\sigma_{i+1,i}^2}\right). \end{aligned} \quad (6)$$

The above approximation holds when  $\sigma_{i+1,i} \gg \Delta t$ ; remember also that  $g_{h,k} = g_{k,h}$ . The  $(M+1) \times (M+1)$  state transition matrix  $\mathbf{A} = [a_{h,k}]$  is normalized along rows; therefore,  $\forall h, k = 1, \dots, M$  the global transition probabilities  $a_{h,k}$  are obtained from  $g_{h,k}$  according the following equation:

$$a_{h,k} = \frac{(1-\nu)g_{h,k}}{\sum_{j=1}^M g_{h,j}}. \quad (7)$$

The truncation due to the finite number of time-cells can cause edge effects in normalization (7) and the diagonal elements  $a_{k,k}$  become dependent on  $k$  (unbalanced gate) [10]. When  $\sigma_{i+1,i} > \Delta t$  the cells on the edge of the observation window have the largest self-transition probabilities. This problem can be avoided by changing the normalization in (7) according to [11]:  $a_{h,k} = (1-\nu)g_{h,k}/g_{\max}$ , where  $g_{\max} = \max_{h \geq 1} \left\{ \sum_{j=1}^M g_{h,j} \right\}$ . This solution implies that  $\sum_{j=0}^M a_{h,j} < 1$ , i.e., there exist further states never occupied by the chain. Note that the transition probabilities  $\{a_{h,k}\}$  do not depend on the SNR of the data as they model only the variability of the wavefield across the sensors.

The initial state distribution is defined by assigning for  $h = 0, 1, \dots, M$  the set of probabilities  $\pi = \{\pi_h\}$ , where  $\pi_h = p[\tau_1 = T_h]$ . The choice of these probabilities depends on the application. For instance, the chain can be forced to start from the null state  $T_0$ :  $\pi_k = a_{0k}$ . Alternatively, if the delay  $\tau(\mathbf{x}_1)$  is known to be  $\tau_1 = T_h$  then it is  $\pi_h = 1$  and  $\pi_k = 0 \forall k \neq h$ .

The specific application considered in this paper requires an HMM with real-valued measurement vectors,  $\mathbf{d}_i \in \mathbb{R}^M$ , differently from the HMM tracking methods usually proposed in the literature where a finite number of possible measurements are considered. Moreover, it is assumed that the observations  $\mathbf{d}_i$  are statistically independent. The probability density function (pdf) of the observation associated with the state  $T_k$  is denoted by  $b_k(\mathbf{d}_i) = p[\mathbf{d}_i | \tau_i = T_k]$  and according to the model (1) is [12]

$$b_k(\mathbf{d}_i) = \begin{cases} \Gamma_i \exp\left(\rho c_i \frac{\phi_{dw}(\mathbf{x}_i, T_k)}{E_w} - c_i^2 \frac{\rho}{2}\right), & k \neq 0 \\ \Gamma_i, & k = 0 \end{cases} \quad (8)$$

where  $\Gamma_i$  is a normalization term.  $\phi_{dw}(\mathbf{x}_i, T_k)$  is the cross-correlation between measured data  $\mathbf{d}_i$  and waveform  $\mathbf{w}(t)$  delayed by  $k\Delta t$  as the most representative delayed signature for the state  $T_k$ . The pdf of the measurement depends on the SNR  $\rho$ , considered here as a free parameter. The amplitude  $c_i$  can be estimated (after tracking) according to the ML criterion:  $\hat{c}_i = \phi_{dw}(\mathbf{x}_i, T_k)/E_w$ .

In the following, the set of parameters of the HMM is indicated with the compact notation  $\boldsymbol{\lambda} = (\mathbf{A}, \mathbf{B}, \pi)$  where  $\mathbf{B}$  is the observation density set defined as  $\mathbf{B} = \{b_k(\cdot)\}$ .

## B. Tracking Algorithms

Either local or global optimality criteria can be adopted to track the optimum state sequence  $\{\hat{\tau}_i\}_{i=1}^N$  given the set of HMM parameters  $\boldsymbol{\lambda}$  (supposed known) and the overall observations  $\mathbf{D}_N = [\mathbf{D}_i, \check{\mathbf{D}}_{i+1}]$ . In the following part of the paragraph,  $\mathbf{D}_N$  is split into two subsets  $\mathbf{D}_i = [\mathbf{d}_1, \dots, \mathbf{d}_i]$  and  $\check{\mathbf{D}}_{i+1} = [\mathbf{d}_{i+1}, \dots, \mathbf{d}_N]$ .

1) *Local Criteria*: If a local criterion is assumed, the sequence is composed of those states  $\hat{\tau}_i$  that are individually most likely given any specific subset  $\mathcal{D}_i$  defined below. For each scan  $\mathbf{x}_i$  the delay  $\tau_i$  is estimated from the *a posteriori* probability mass (or density) function  $\gamma_i(k) = p[\tau_i = T_k | \mathcal{D}_i, \boldsymbol{\lambda}]$  according to the MAP or MMSE criterion

$$\hat{\tau}_i|_{\text{MAP}} = \Delta t \arg \max_{1 \leq k \leq M} \gamma_i(k), \quad 1 \leq i \leq N \quad (9)$$

$$\hat{\tau}_i|_{\text{MMSE}} = \frac{\Delta t \sum_{k=1}^M k \gamma_i(k)}{\sum_{k=1}^M \gamma_i(k)}, \quad 1 \leq i \leq N. \quad (10)$$

The Detection/Tracking Algorithm (D/TA) [12] is based on this local criterion with  $\mathcal{D}_i = \mathbf{D}_i$ . The optimum sequence is the one that, for each location  $\mathbf{x}_i$ , maximizes the *a posteriori* probability of the delay given the signals measured up to the specified location  $\mathbf{x}_i$ :  $\gamma_i(k) = p[\tau_i = T_k | \mathbf{D}_i, \boldsymbol{\lambda}]$ . From Bayes' theorem the *a posteriori* pdf in  $\mathbf{x}_{i+1}$  can be written as

$$\gamma_{i+1}(k) = \mu_{i+1} p[\mathbf{d}_{i+1} | \tau_{i+1} = T_k, \boldsymbol{\lambda}] p[\tau_{i+1} = T_k | \mathbf{D}_i, \boldsymbol{\lambda}] \quad (11)$$

where  $\mu_{i+1}$  is a normalization term for  $\gamma_{i+1}(k)$ :  $\sum_{k=0}^M \gamma_{i+1}(k) = 1$ . The conditional pdf of the observation  $b_k(\mathbf{d}_{i+1}) = p[\mathbf{d}_{i+1} | \tau_{i+1} = T_k, \boldsymbol{\lambda}]$  is obtained as described in Section III-A, while the *a priori* pdf  $p[\tau_{i+1} = T_k | \mathbf{D}_i, \boldsymbol{\lambda}]$  can be calculated

TABLE I  
TRACKING ALGORITHMS BASED ON LOCAL (DETECTION/TRACKING ALGORITHM) AND GLOBAL (BACKWARD-FORWARD AND VITERBI ALGORITHM) CRITERIA

	INITIALIZATION	RECURSION
<b>D/TA</b>	$\gamma_1(k) = \mu_1 \pi_k b_k(\mathbf{d}_1)$	$\gamma_{i+1}(k) = \mu_{i+1} b_k(\mathbf{d}_{i+1}) \sum_{h=0}^M a_{hk} \gamma_i(h)$
<b>BFA</b>	$\alpha_1(k) = \pi_k b_k(\mathbf{d}_1)$ $\beta_N(k) = 1$	$\alpha_{i+1}(k) = b_k(\mathbf{d}_{i+1}) \sum_{h=0}^M \alpha_i(h) a_{hk}$ $\beta_i(k) = \sum_{h=0}^M a_{kh} b_h(\mathbf{d}_{i+1}) \beta_{i+1}(h)$
<b>VA</b>	$\delta_1(k) = \pi_k b_k(\mathbf{d}_1)$ $\zeta_1(k) = 0$	$\delta_{i+1}(k) = b_k(\mathbf{d}_{i+1}) \max_{0 \leq h \leq M} \{\delta_i(h) a_{hk}\}$ $\zeta_{i+1}(k) = \arg \max_{0 \leq h \leq M} \{\delta_i(h) a_{hk}\}$

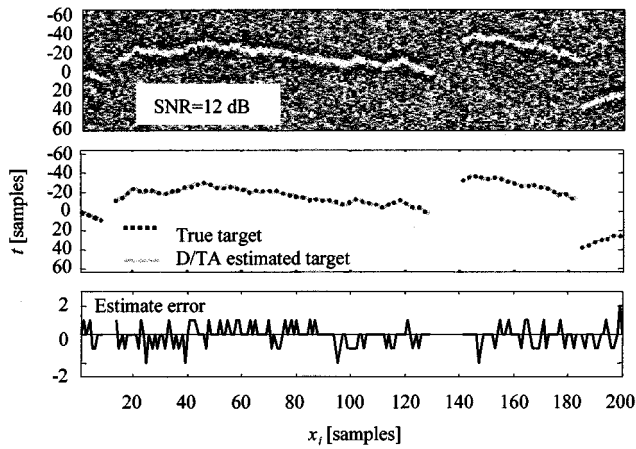


Fig. 3. Example of single target D/TA estimation. From top to bottom: observations (top) generated by an HMM [SNR = 2 dB,  $\vartheta = 0.1$ ,  $v = 0.01$ ,  $\sigma_{i+1,i} = 1.6$ ,  $c_i = 1$ ,  $M = 128$ ]; estimated delay function (MAP criteria) compared with the actual one (center) [the parameters of the Markov model are known to the tracker]; the estimation error (bottom).

from the *a posteriori* pdf for the previous space location  $\mathbf{x}_i$  by the transition probabilities of the Markov chain

$$p[\tau_{i+1} = T_k | \mathbf{D}_i, \lambda] = \sum_{h=0}^M a_{hk} p[\tau_i = T_h | \mathbf{D}_i, \lambda] = \sum_{h=0}^M a_{hk} \gamma_i(h). \quad (12)$$

Remember that for nonuniform sensor spacing, the transition probability  $a_{h,k}$  from (6) depends on the distance between the two consecutive sensors  $\|\mathbf{x}_{i+1} - \mathbf{x}_i\|$ . Substitution of (12) into (11) yields the recursive procedure for the calculation of  $\gamma_i(k)$  as summarized in Table I. The D/TA is a forward procedure, as the estimation of  $\tau_i$  is based only on measurements up to the  $i$ th scan ( $\mathbf{D}_i$ ), whereas the remaining observations from the  $(i+1)$ th scan up to the end are not taken into account. This makes the algorithm suitable for real-time applications as the delay can be obtained directly at the  $i$ th step without latency. An example of D/TA is shown in Fig. 3 for a single target ( $L = 1$ ) and SNR = 12 dB. The waveform  $w(t)$  is the second-order derivative of a Gaussian pulse,  $w(t) = (1 - t^2/T_w^2) \exp(-t^2/2T_w^2)$ ,

as this signal is representative of the waveforms used in applications related to subsurface sensing (here  $T_w = 4$  samples). The target is properly detected and tracked even if the initiation and termination probabilities are set to values that make the delays discontinuous across the space locations.

2) *Global Criteria*: In global criteria methods, the whole set of available measurements  $\mathcal{D}_i = \mathbf{D}_N$  is taken into account. The optimum sequence of states is obtained by maximizing the *a posteriori* probability  $\gamma_i(k) = p[\tau_i = T_k | \mathbf{D}_N, \lambda]$  for all the measurements  $\mathbf{D}_N$ . This maximization can be carried out on a scan by scan basis as for the Backward-Forward Algorithm (BFA) or by searching the optimum sequence of states as for the Viterbi Algorithm (VA). Sometimes (see e.g., [15]) the BFA is considered a local criterion because it locally maximizes the term  $\gamma_i(k)$ . However, we want to stress the fact that all the measurements need to be processed to obtain  $\gamma_i(k)$ .

The *a posteriori* pdf  $\gamma_i(k)$  depends on both the backward probabilities  $\alpha_i(k) = p[\mathbf{D}_i, \tau_i = T_k | \lambda]$  and the forward probabilities  $\beta_i(k) = p[\mathbf{D}_{i+1} | \tau_i = T_k, \lambda]$

$$\gamma_i(k) = \frac{\alpha_i(k) \beta_i(k)}{\sum_{h=0}^M \alpha_i(h) \beta_i(h)}, \quad \text{for } k = 0, \dots, M. \quad (13)$$

In the BFA, each of the probabilities can be calculated recursively, and separately, by starting from the beginning and the end of the dataset (see Table I) in a fashion similar to the D/TA.

Both the D/TA and the BFA estimate the most likely delay at each scan regardless of the sequence of states, hence the resulting target could be far from being plausible. This easily occurs when multiple targets get close to each other (e.g., below the time-resolution of the signature  $w(t)$ ) and tracked targets jump almost without control. This inconvenience is compensated by the VA [16] that estimates the optimum state sequence by maximizing  $p[\tau_1, \tau_2, \dots, \tau_N | \mathbf{D}_N, \lambda]$ , or equivalently  $p[\tau_1, \tau_2, \dots, \tau_N, \mathbf{D}_N | \lambda]$ . In practice, at the  $i$ th scan, the optimum state sequence is the one that having the delay  $\tau_i = T_k$  maximizes the joint probability of the state sequence and the measurement set  $\mathbf{D}_i$

$$\delta_i(k) = \max_{\tau_1, \tau_2, \dots, \tau_{i-1}} \{p[\tau_1, \tau_2, \dots, \tau_i = T_k, \mathbf{D}_i | \lambda]\}. \quad (14)$$

The probabilities  $\delta_i(k)$  can be calculated recursively as in Table I [15] and the functions  $\zeta_i(k)$  keep track of the optimum state sequence. The algorithm stops when the  $N$ th iteration is performed:  $\hat{\tau}^*(x_N) = \arg \max_{0 \leq h \leq M} \delta_N(h)$ . The optimum state sequence is reversely obtained for  $i = N-1, i = N-2, \dots, i = 1$  from the backtracking equation  $\hat{\tau}_i^* = \zeta_{i+1}(\hat{\tau}_{i+1}^*)$ . The delays are evaluated accordingly as  $\hat{\tau}_i = \Delta t \cdot \hat{\tau}_i^*$ . The computation of the sequence for BFA and VA requires about  $N(M+1)^2$  calculations [15].

#### IV. MULTIDIMENSIONAL DELAY TRACKING ( $n > 1$ )

The wavefield is obtained by sources/receivers placed almost irregularly in the  $n$ -D space. Therefore, data ordering becomes the main issue in exploiting the efficient delay tracking algorithm discussed previously. Our aim is to order the scans dynamically while tracking. Let  $\mathcal{R}_i = \{\mathbf{x}_1, \dots, \mathbf{x}_i\}$  be the set

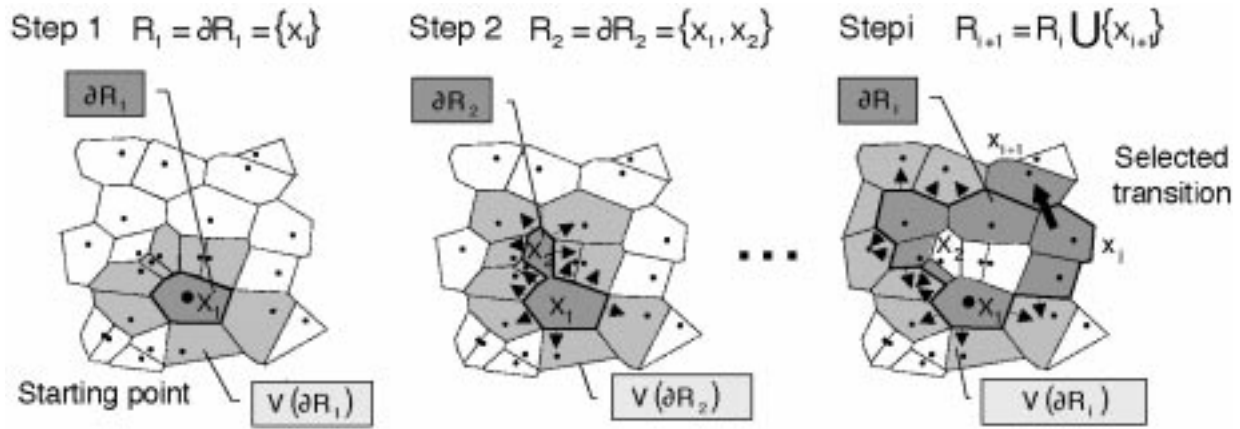


Fig. 4. Region growing algorithm. From top to bottom: first iteration (left); from the starting point  $\{x_1\}$  the tracking grows into the point  $x_2 \in \mathcal{V}(\{x_1\})$ . Second iteration (center) redefines the boundary  $\mathcal{V}(\{x_1, x_2\})$  and selects one point with the largest *a posteriori* detection probability. At the *i*th step (right) the region  $R_i = \{x_1, \dots, x_i\}$  grows by the selection of the transition  $x_j \rightarrow x_{i+1}$  where  $x_j \in \partial R_i$  and  $x_{i+1} \in \mathcal{V}(\partial R_i)$ .

of the points already tracked at the *i*th step,  $\partial R_i$  denotes the boundary of  $R_i$ ,  $\mathcal{V}(x_j)$  is the neighboring set of  $x_j$  for any  $x_j \in \partial R_i$ . The tracking grows by selecting from the neighborhood  $\mathcal{V}(\partial R_i)$  of  $\partial R_i$  the next scan  $d_{i+1}$  in  $x_{i+1}$  that has the most likely delay compared to the delays already estimated. The cost function adopted for this region growing algorithm is based on the *a posteriori* pdf for the underlined HMM. Note that the location ordering reflects the ordering of the tracking.

The choice of  $\mathcal{V}(\partial R_i)$  is made to restrict the tracking to the most likely subset where the target preserves its similarities with the targets in  $R_i$ . Since the transition probabilities (6) depend on the distance between the two sensors, the *a priori* information in the tracking algorithm can easily become noninformative when the selection  $\mathcal{V}(\partial R_i)$  is far from any sensor in  $\partial R_i$ . In this case, the delay estimation approaches the maximum likelihood estimate. Any reasonable strategy for the selection of  $\mathcal{V}(\partial R_i)$  based on neighboring selection is equally valid, we propose the use of Delaunay triangulation [17].

#### A. Region Growing Tracking

Details on the tracking strategies are given by illustrating an example in Fig. 4, for  $n = 2$  dimensions. Let us consider one starting point  $x_1$ , the initial set is  $R_1 = \partial R_1 = \{x_1\}$ , the neighborhood  $\mathcal{V}(\partial R_1)$  can be obtained from Delaunay triangulation. Among the scans  $d_k$  with  $x_k \in \mathcal{V}(\{x_1\})$  the selection is made according to the *a posteriori* pdf as specified below. The new set now becomes  $R_2 = \partial R_2 = \{x_1, x_2\}$  and the neighboring points  $\mathcal{V}(\partial R_2)$  are obtained accordingly.

At the *i*th step (Fig. 4) the algorithm searches for a further point  $x_{i+1} \in \mathcal{V}(\partial R_i)$  to include in the set  $R_i$ . For this purpose the *a posteriori* probability of detection needs to be assessed for any transition  $x_j \rightarrow x_m$  from the boundary  $\partial R_i$  to the neighborhood  $\mathcal{V}(\partial R_i)$ , i.e., for any  $(x_j, x_m)$  with  $x_j \in \partial R_i$  and  $x_m \in \mathcal{V}(x_j)$ . The new point  $x_{i+1}$  is obtained by selecting from all the allowed transitions the one with the largest *a posteriori* probability

$$x_{i+1} = \arg \max_{x_j \in \partial R_i, x_m \in \mathcal{V}(x_j)} p[H_1(x_m) | \mathbf{D}_j, \mathbf{d}_m, \lambda] \quad (15)$$

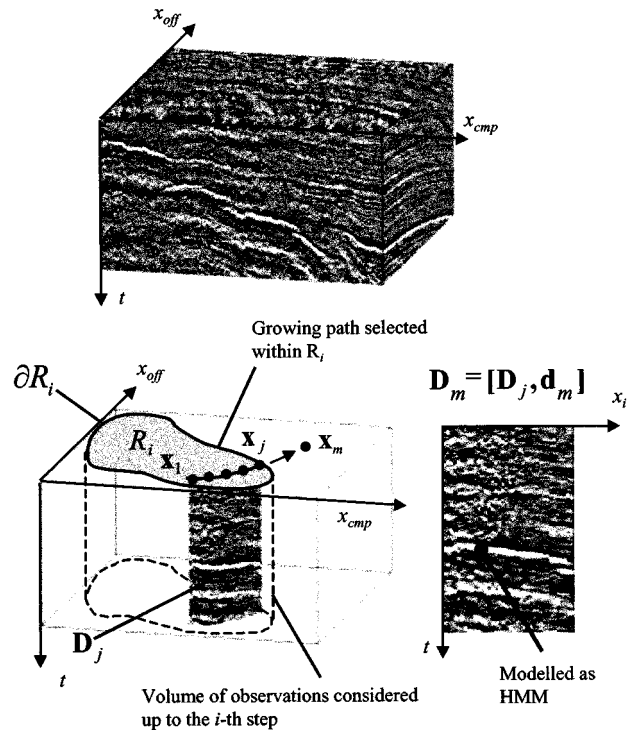


Fig. 5. Region growing tracking along a path for 3-D data volume,  $n = 2$  ( $x_{cmp} = (x_s + x_r)/2$  is the mid point coordinate,  $x_{off} = x_s - x_r$  is the source-receiver offset). From top to bottom: 3-D data volume (top). D/TA is performed (bottom left) for  $x_j \rightarrow x_m$  in order to assess the *a posteriori* pdf of  $\tau(x_m)$  given the sequence of observations  $[\mathbf{D}_j, \mathbf{d}_m]$  associated with the growing path up to  $x_m$  (bottom right).

where  $\mathbf{D}_j$  is the sequence of observations associated with the growing path that starts in  $x_1$  and end up in  $x_j \in \partial R_i$ , as illustrated in Fig. 5. Note that, in general, this path is not equal to  $[x_1, \dots, x_j]$ . The cost function  $p[H_1(x_m) | \mathbf{D}_j, \mathbf{d}_m, \lambda]$  used for the selection is the *a posteriori* probability that a target is present in  $x_m$  (regardless of the delay) given the observations  $\{\mathbf{D}_j, \mathbf{d}_m\}$  up to  $x_m$ . The point selected by (15) is then included in the region  $R_{i+1} = R_i \cup \{x_{i+1}\}$  and the procedure is iterated on the new boundary  $\partial R_{i+1}$  for the selection of  $x_{i+2}$ .

In this way every step is performed by making the region  $R_i$  grow along the paths where the targets can be more easily

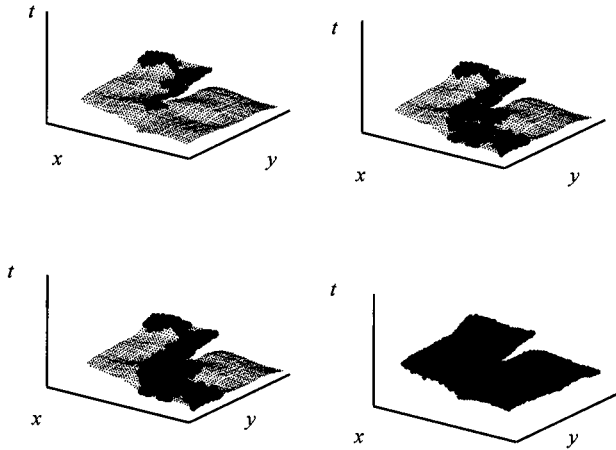


Fig. 6. Iterative region growing algorithm. From top to bottom and left to right: iterations of region growing algorithm around a faulty area (same parameters as the example in Fig. 3).

predicted according to the *a posteriori* detection criteria (15). The algorithm terminates when the whole horizon has been estimated, i.e., when  $i = N$ ,  $\mathcal{R}_N = \{\mathbf{x}_1, \dots, \mathbf{x}_N\}$  and  $\partial\mathcal{R}_N$  is empty.

The *a posteriori* probability in (15) can be assessed by modeling the delay function along the growing path as an HMM  $\lambda$  and then applying the D/TA to the set of observations associated with the path (see Fig. 5)

$$\begin{aligned} p[H_1(\mathbf{x}_m)|\mathbf{D}_j, \mathbf{d}_m, \lambda] &= \sum_{k=1}^M p[\tau(\mathbf{x}_m) = T_k | \mathbf{D}_j, \mathbf{d}_m, \lambda] \\ &= \mu_m \sum_{k=1}^M b_k(\mathbf{d}_m) \sum_{h=0}^M a_{hk} \gamma_j(h). \end{aligned} \quad (16)$$

$\mu_m$  is a normalizing term,  $\gamma_j(h) = p[\tau(\mathbf{x}_j) = T_h | \mathbf{D}_j, \lambda]$  is the *a posteriori* pdf of the delay in  $\mathbf{x}_j$ .

In summary, the steps of the  $n$ -D tracking based on the region growing are the following: 1) search for the neighboring points  $\mathcal{V}(\partial\mathcal{R}_i)$  of the boundary of  $\mathcal{R}_i$ ; 2) evaluate the *a posteriori* probabilities  $p[H_1(\mathbf{x}_k)|\mathbf{D}_j, \mathbf{d}_m, \lambda]$  for all the possible transitions  $\mathbf{x}_j \rightarrow \mathbf{x}_m$  with  $\mathbf{x}_j \in \partial\mathcal{R}_i$  and  $\mathbf{x}_m \in \mathcal{V}(\mathbf{x}_j)$ ; and 3) select the largest value, estimate the corresponding delay according to any of the aforementioned MAP or MMSE criteria (9–10), update the sets  $\mathcal{R}_{i+1} = \{\mathcal{R}_i, \mathbf{x}_{i+1}\}$  and  $\partial\mathcal{R}_{i+1}$ . In this way data ordering is obtained implicitly and the 1-D tracking strategies previously discussed can be exploited.

This iterative approach has no proof of global optimality even if the wavefront is estimated by collecting locally optimum selections. Neighboring selection criteria can be proved to be optimum when estimates with greater distances are obtained from a sequence of estimates with shorter distances (see the Appendix). However, the region growing tracking has proved to be effective in estimating horizon with discontinuities (e.g., faults) or low SNR areas. If the horizon is connected in the  $(n + 1)$ -D volume, the tracking grows along the largest continuity paths that go around the discontinuities as the *a posteriori* probability  $p[H_1(\mathbf{x}_i)|\mathbf{D}_i, \lambda]$  is usually very low

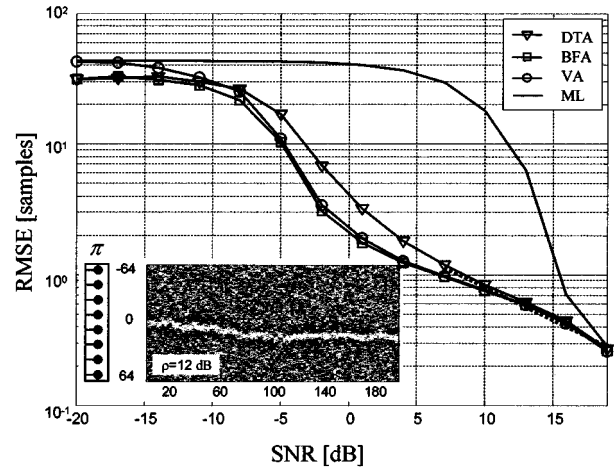


Fig. 7. Performance of HMM single-target algorithms in terms of RMSE versus SNR ( $n = 1$ ). RMSE for maximum-likelihood (ML) estimate is superimposed as reference.

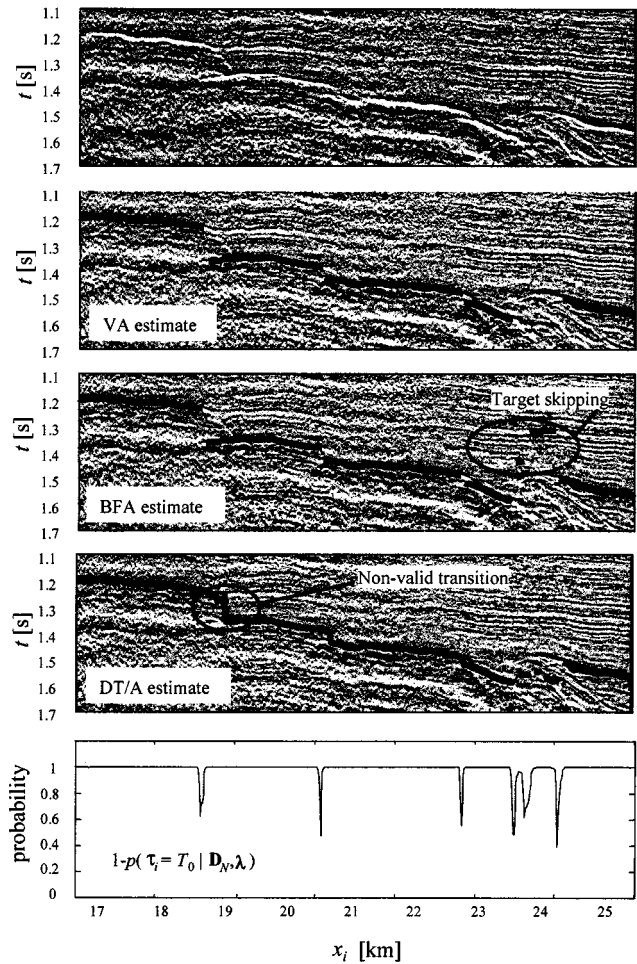


Fig. 8. Example from field data (the volume is sliced as common offset section so that  $n = 1$ ). The parameters of HMM trackers are estimated from the data, the initial position of the target is given. From top to bottom: data (top); VA estimate; BFA estimate; D/TA estimate; *a posteriori* probability of detection for the BFA (bottom).

when the transition occurs across a faulty area (see example in Fig. 6). Extension to multiple target can be employed by a recursive approach; see [12] for a discussion.

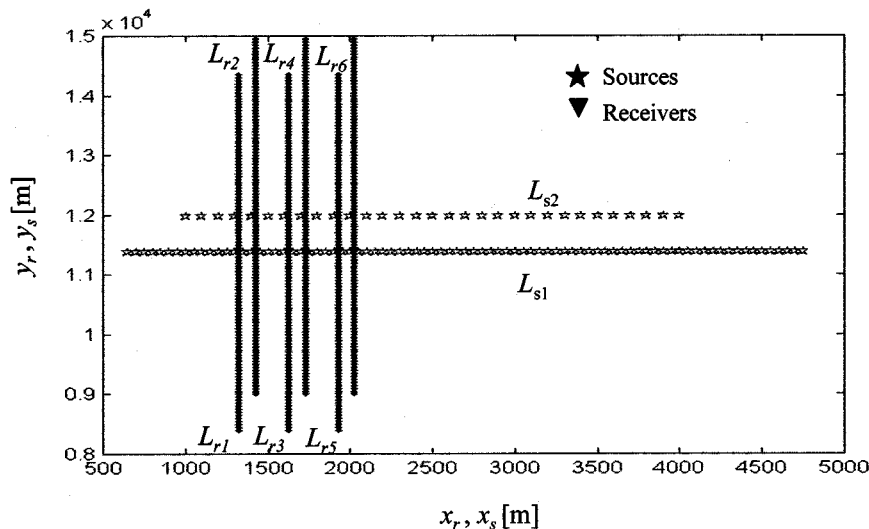


Fig. 9. Acquisition geometry from the SEG-EAEG 3-D overthrust model. The data volume is shown in Fig. 10.

### B. Region Growing Implementation

The region growing tracking requires to store in memory the *a posteriori* probability  $p[\tau(\mathbf{x}_m) = T_k | \mathbf{D}_j, \mathbf{d}_m, \boldsymbol{\lambda}]$  for all the paths that end at the boundary, i.e., for  $\mathbf{x}_j \in \partial\mathcal{R}_i$  and  $\mathbf{x}_m \in \mathcal{V}(\mathbf{x}_j)$ . The growing algorithm can be efficiently implemented by using a data structure based on the height-balanced binary search tree (AVL tree) [18]. The selection of  $\mathbf{x}_{i+1}$  at step  $i$  requires the evaluation and maximization of the *a posteriori* probabilities associated with all the transitions  $\mathbf{x}_j \rightarrow \mathbf{x}_m$  (15). Therefore, the statistical information that needs to be stored for the growing is only that related to the points on the boundary and to the corresponding neighbors: the probabilities  $p[H_1(\mathbf{x}_m) | \mathbf{D}_j, \mathbf{d}_m, \boldsymbol{\lambda}]$  and the *a posteriori* probability  $\gamma_m(k) = p[\tau(\mathbf{x}_m) = T_k | \mathbf{D}_j, \mathbf{d}_m, \boldsymbol{\lambda}]$  (for the next growing steps). This information can be stored in an AVL tree as such a structure reduces the time of search, insertion and deletion operations to  $O(\ln |\partial\mathcal{R}_i|)$ , where  $|\cdot|$  denotes the cardinality of the set. Each node in the tree corresponds to a point on the boundary  $\mathbf{x}_j \in \partial\mathcal{R}_i$ , the search-key is the maximum of the probabilities  $p[H_1(\mathbf{x}_m) | \mathbf{D}_j, \mathbf{d}_m, \boldsymbol{\lambda}]$  for all the neighbors  $\mathbf{x}_m \in \mathcal{V}(\mathbf{x}_j)$ ; the node data are the cost values  $p[H_1(\mathbf{x}_m) | \mathbf{D}_j, \mathbf{d}_m, \boldsymbol{\lambda}]$  and the pdfs  $\gamma_m(k)$  for any  $\mathbf{x}_m \in \mathcal{V}(\mathbf{x}_j)$ .

## V. PERFORMANCE AND EXAMPLES

The performance of the tracking algorithms (D/TA, BFA, VA) are compared in Fig. 7 in terms of root mean square error (RMSE) of the estimated delays versus SNR (same HMM parameters as for the example in Fig. 3 without initiation and termination:  $\nu = \vartheta = 0$ ). The tracking methods based on global criteria (BFA and VA) have similar performance when evaluated around the threshold region (for SNR in the range  $-10$ – $10$  dB) and show meaningful advantages (approx. 3 dB in SNR) compared to D/TA. For larger SNR, all the methods have comparable RMSE and attain the Cramèr–Rao bound (dotted line) as for the cross-correlation estimator (or maximum likelihood estimator) based on the search for delay where the  $\phi_{dw}(\mathbf{x}_i, T_k)$  peaks. However, target initiation or termination

are not reliable without the implicit memory given by the tracking algorithms.

The advantages of VA over others can be appreciated from a comparison of the tracking algorithms over faulty seismic data in Fig. 8; the data are sliced as common offset sections to have  $n = 1$  almost uniformly spaced data. In this case the HMM parameters are estimated from the data itself, the parameters used for tracking are: SNR = 5 dB,  $L = 1$ ,  $\vartheta = 0.2$ ,  $\nu = 0.01$ ,  $\sigma = 1.6$ ,  $c_i = 1$ ,  $M = 140$ ,  $N = 701$ , the initial position of the target is known. The delay functions estimated on the base of locally optimum criteria (BFA and D/TA) show skipping between different targets, for the BFA the delays show state transitions that are unlikely. Even if the VA preserve the association between target and tracker, the extension to handle multidimensional dataset ( $n > 1$ ) is computationally expensive. However, examples below show that the exploitation of the continuity of the target when considered globally from multidimensional data makes the problem of target skipping much less severe than for  $n = 1$ .

The robustness of multidimensional tracking to track targets within the 5-D data volume from seismic dataset is considered now. The experimental data comes from the SEG/EAEG 3-D Overthrust model [19]. Two different layouts for the acquisition are considered, each leading to a partially-regular source/receiver spacing. In the first example (Fig. 9) the sources are arranged along two lines indicated here as  $L_{s1}$  and  $L_{s2}$ , sources along the  $L_{s2}$  line have double spacing compared to  $L_{s1}$ . Backscattered wavefield from each source in  $L_{s1}$ , or  $L_{s2}$ , is recorded by three different arrays of receivers arranged along lines:  $L_{r1}$ ,  $L_{r3}$ ,  $L_{r5}$  for sources along  $L_{s1}$  and  $L_{r2}$ ,  $L_{r4}$ ,  $L_{r6}$  for sources along  $L_{s2}$ . The received signals are time sampled with  $\Delta t = 8$  ms. Each source–receiver pair is identified by the set  $\mathbf{x} = (x_s, y_s, x_r, y_r)$ , where  $(x_s, y_s)$  and  $(x_r, y_r)$  are the spatial coordinates of the source and the receiver, respectively. Therefore, it is  $n = 4$  and the set of observations represents a 5-D data volume  $d(x_s, y_s, x_r, y_r, t)$ . Fig. 10 shows the data volume and the D/TA estimate for a single wavefront (HMM parameters:  $\sigma = 4.6$  ms,  $\vartheta = \nu = 0.2$ ,  $\rho = 12$  dB). The estimated 4-D hyper-surface is shown for

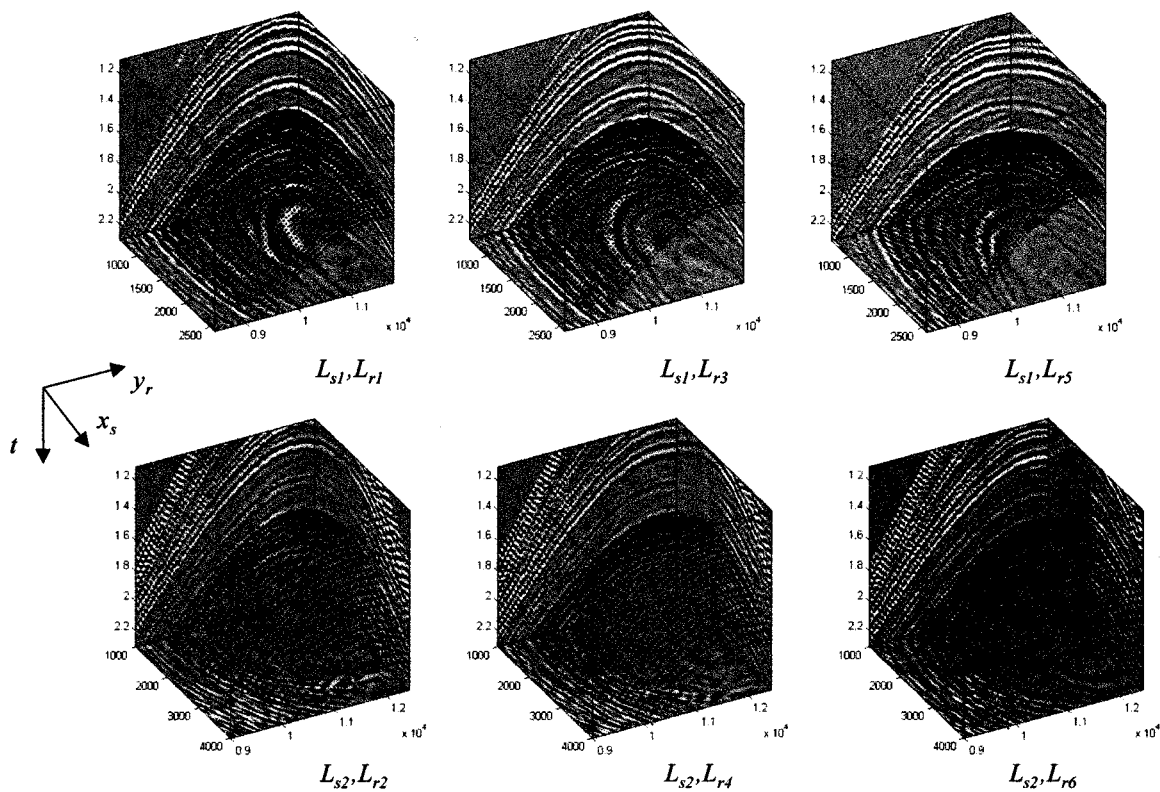


Fig. 10. Estimate of  $\tau(x_s, y_s, x_r, y_r)$  from the 5-D set of signals measured by the source/receiver arrangement in Fig. 9. Each figure shows the delays of the wavefront for the couple source line/receiver line (or  $y_s = \text{const}$  and  $x_r = \text{const}$ ).

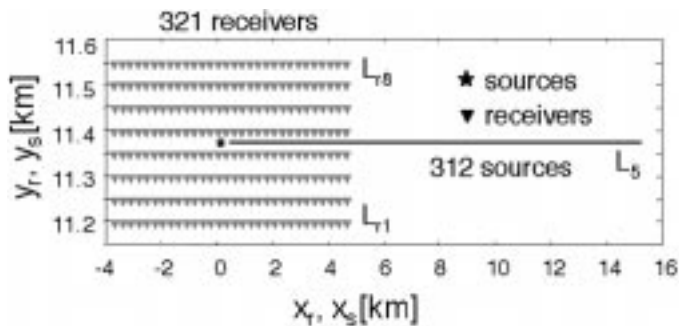


Fig. 11. Acquisition geometry from the SEG-EAEG 3-D Overthrust Model: receivers are arranged as 2-D array and sources are along a line (a 3-D subset of the data volume is shown in Fig. 12).

fixed values of  $y_s$  and  $x_r$  thus having the six 2-D surfaces  $\tau(x_s, \bar{y}_s = \text{const}, \bar{x}_r = \text{const}, y_r)$  corresponding to the six pair source line/receiver line. The delay surfaces are close to the horizons that appear from the slices of the seismic volumes, and are never misaligned on different targets, as it could occur when tracking is performed separately on different subsets. Delays are continuous as this dataset is far from the faulty area.

The example in Fig. 12 refers to the same SEG/EAEG 3-D Overthrust model but with a different acquisition geometry (Fig. 11). Sources are arranged along the line  $L_s$ , the receivers along 6 lines  $L_{r1}$ – $L_{r6}$  to get a 2-D planar array. The 3-D subset shown in Fig. 12 is extracted from the data volume by selecting the lines  $L_s$  and  $L_{r1}$ . Fig. 12 shows three faulted horizons estimated by D/TA that closely preserve the association with the targets. Multidimensional tracking has the advantage that

the target/tracker association can be preserved by going round the discontinuous areas and thus maintaining the association in all the dimensions simultaneously. The values of the  $a$  *a posteriori* probability of detection for the three targets are at the bottom of Fig. 12. The values are higher in the flat area (or equivalently where the target can be more easily predicted from its neighboring points), lower around the faults and in the area where the wavefront is increasing.

Another example from field data (2-D marine seismic experiment) is shown in Fig. 13, together with four steps from the region growing tracking (in this case the data volume is 3-D). The regions grow from the seed points, thus filling all the faulted surfaces. Two slices are shown in Fig. 14.

By comparing the example in Fig. 8 with the same tracking parameters it can be seen that the multidimensional D/TA preserves the association with the target, similarly to the VA algorithm.

*Remark:* The Markov model can be used to describe the random component of the backscattered wavefields. This implies that any deterministic component needs to be compensated before tracking. Standard compensations (also referred to as moveout corrections [13]) depend on propagation velocity that is known with a large degree of uncertainty. The accuracy of this compensation is not critical but it does improve the accuracy and target/tracker association. In the examples shown here moveout corrections have not been applied.

## VI. CONCLUSIONS

Inspired by the fractal description of terrains we have demonstrated that the delays of backscattered wavefields

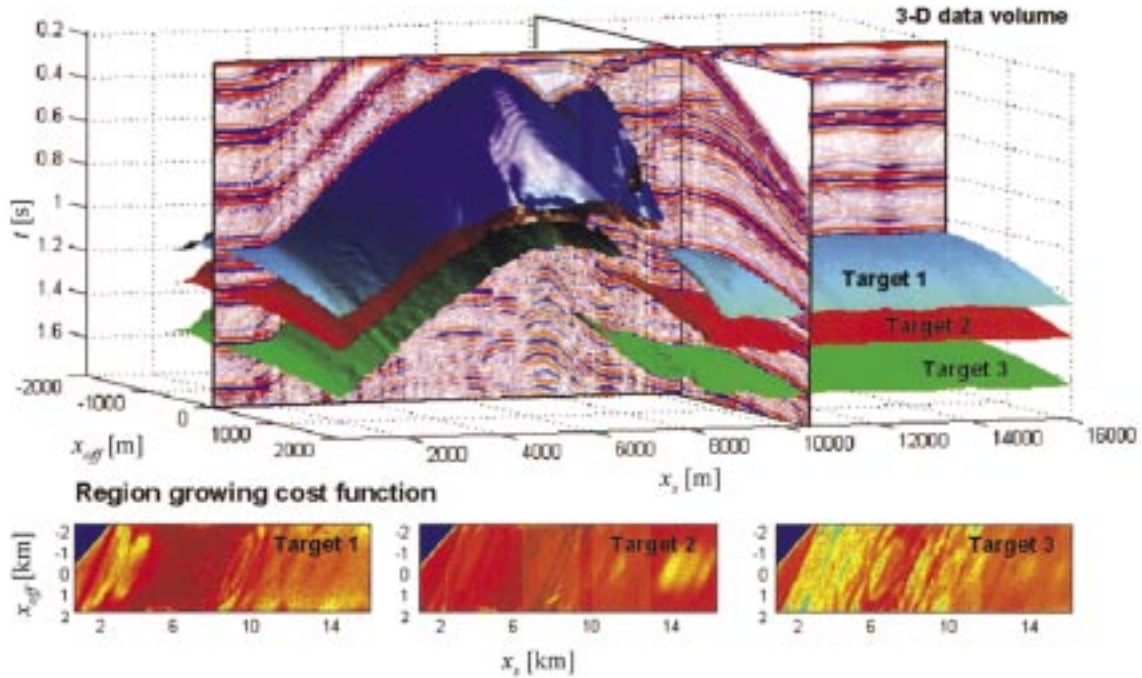


Fig. 12. Multitarget estimation by D/TA. From top to bottom: a subset of the 5-D measurement set is shown by extracting the receiver line  $L_{r-1}$  and the source line  $L_s$  (offset is the distance between source and receiver) in Fig. 11 (top). Three faulted horizons estimated by D/TA are superimposed with the dataset still preserving the association with the target. The cost function values of the region growing path are shown for each of the three targets (bottom).

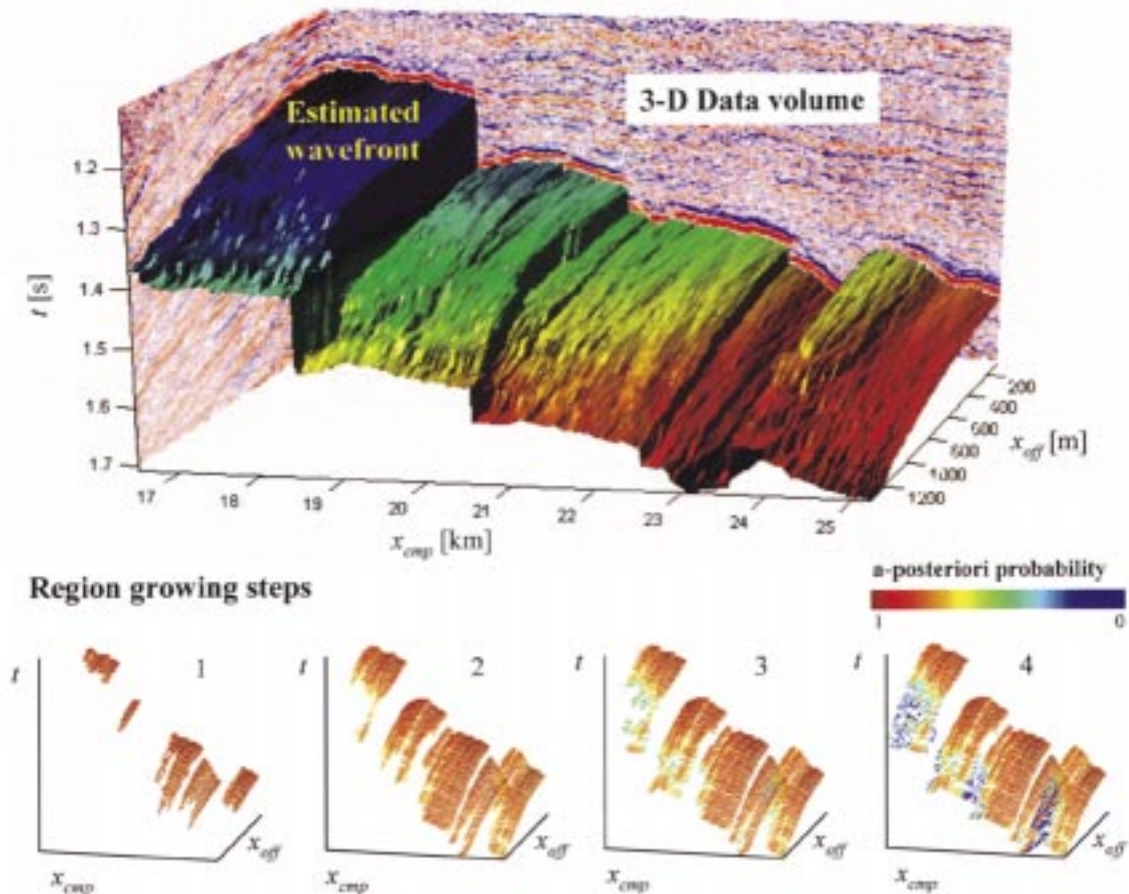


Fig. 13. Example of faulted horizon tracking for 2-D marine seismic experiment ( $x_{cmp}$  is the midpoint coordinate and  $x_{off}$  is the offset). The estimated wavefront for one of the targets of interest is superimposed on the 3-D data volume (here sliced only for visualization). Bottom figures: four snapshots of the delay surfaces for four region growing steps, the values of the *a posteriori* probability of detection are superimposed in color coding.

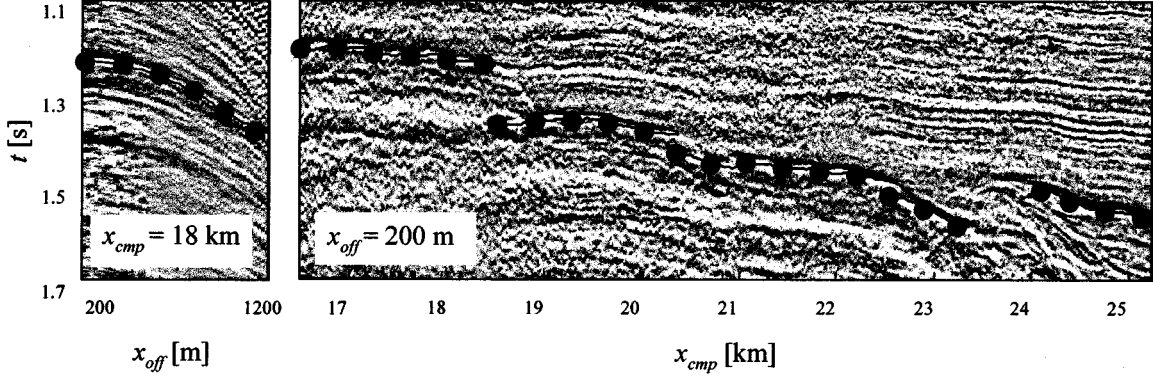


Fig. 14. Common source ( $x_{\text{comp}} = 18$  km) and common offset sections ( $x_{\text{off}} = 200$  m). From left to right: common source (left) and common offset (right) sections from the dataset described in Fig. 13.

can be tracked by modeling the wavefronts as random processes (Brownian motion) with correlation properties that depend on the distance of source/receiver pairs. The sequence of states of the Markov model can be tracked by any of the known methods for the estimation of sequence of states. Even if the detection/tracking algorithm is based on a local criterium, it is accurate enough for most practical purposes, and it does not need of both causal/anticausal scans for delay estimation. In practical applications the ordering of the data acquired with irregular source/receiver positioning is not an easy task. Region growing techniques provide data-ordering, while the tracking of the targets is based on the local maximization (at each step) of the *a posteriori* probability of detection. Compared to methods that slice the multidimensional dataset into ordered sequence and then use sophisticated tracking strategies (e.g., Viterbi algorithm), region growing tracking based on the detection/tracking algorithm maintains the target/tracker association by efficiently exploiting the multidimensionality of the measurements.

#### APPENDIX

In region growing tracking the estimation of the delays is based on the neighborhood selection criteria; a first order analysis is proposed to support this strategy in a simple case without detection (i.e.,  $T_o = \emptyset$ ). We compare two strategies to reach the point in  $\mathbf{x}_3$  starting from a point in  $\mathbf{x}_1$  with or without transition into a neighboring intermediate point in  $\mathbf{x}_2$ . The alternatives are summarized below as cases 1–2–3:  $\mathbf{x}_1 \rightarrow \mathbf{x}_2 \rightarrow \mathbf{x}_3$  and 1–3:  $\mathbf{x}_1 \rightarrow \mathbf{x}_3$ . Without losing the generality, we assume that  $\|\mathbf{x}_1 - \mathbf{x}_2\| = \|\mathbf{x}_3 - \mathbf{x}_2\| = 1$  and the distance  $z = \|\mathbf{x}_1 - \mathbf{x}_3\| \in (0, 2]$  ( $\mathbf{x}_3$  is closer to  $\mathbf{x}_1$  for  $z \leq 1$  and  $\mathbf{x}_1, \mathbf{x}_2, \mathbf{x}_3$  are aligned in space for  $z = 2$ ). The delay associated with the observation  $\mathbf{d}_i$  at each point  $\mathbf{x}_i$  is constant  $\tau_i = \tau$  (or deviations are small) and the target roughness is described by the variance  $\sigma_{i+1,i}^2 = \sigma^2 \|\mathbf{x}_{i+1} - \mathbf{x}_i\|$ . For high SNR values  $\rho$  and known amplitude  $c_i$ , the cross-correlation  $\phi_{dw}(t)$  in (8) can be approximated around its true value  $\tau$

$$\begin{aligned} \phi_{dw}(t - \tau) &= \phi_{ww}(t - \tau) + \phi_{nw}(t - \tau) \\ &\simeq E_w + \frac{1}{2} \ddot{\phi}_{ww}(0) (t - \tau)^2 \end{aligned} \quad (17)$$

where  $\ddot{\phi}_{ww}(t - \tau)$  denotes the second order derivative of the autocorrelation function. By assuming a diffuse *a priori* information, the *a posteriori* pdf of the estimate  $\hat{\tau}_1$  is

$$p_1 \propto \exp\left(-\frac{(t - \tau)^2}{2\sigma_\phi^2}\right) \quad (18)$$

where  $\sigma_\phi^2 = -\sigma_n^2 / \ddot{\phi}_{ww}(0)$  is the equivalent variance of the conditional pdf (8) for the approximation (17). Two different trajectories are considered when starting from  $\mathbf{x}_1$  and ending in  $\mathbf{x}_3$ , the variance of the *a posteriori* pdf is compared to assess which of them is the most likely.

**Case 1–3:** following the path  $\mathbf{x}_1 \rightarrow \mathbf{x}_3$ , the *a posteriori* pdf of  $\hat{\tau}_3$  is Gaussian with variance  $\sigma_{13}^2$  obtained by composing the *a posteriori* pdf in  $\mathbf{x}_1$  with transition probability:

$$\frac{1}{\sigma_{13}^2} = \frac{1}{z\sigma^2 + \sigma_\phi^2} + \frac{1}{\sigma_\phi^2} = \frac{1}{\sigma_\phi^2} \left(1 + \frac{1}{z\mu + 1}\right) \quad (19)$$

notice that we have used the fractal properties of the transition probability; the term

$$\mu = \frac{\sigma^2}{\sigma_\phi^2} = -\ddot{\phi}_{ww}(0) \cdot \frac{\sigma^2}{\sigma_n^2} > 0 \quad (20)$$

is related to the waveform resolution.

**Case 1–2–3:** following first the path  $\mathbf{x}_1 \rightarrow \mathbf{x}_2$  and then  $\mathbf{x}_2 \rightarrow \mathbf{x}_3$ , exploiting the same approach adopted before, it is easy to show from (19) that the *a posteriori* pdf of  $\hat{\tau}_2$  has variance given by:

$$\frac{1}{\sigma_{12}^2} = \frac{1}{\sigma_\phi^2} \left(1 + \frac{1}{\mu + 1}\right) \quad (21)$$

while the *a posteriori* pdf of estimate  $\hat{\tau}_3$  has variance given by:

$$\frac{1}{\sigma_{123}^2} = \frac{1}{\sigma_{12}^2 + \sigma^2} + \frac{1}{\sigma_\phi^2} = \frac{1}{\sigma_\phi^2} \left(1 + \frac{\mu + 2}{\mu^2 + 3\mu + 1}\right). \quad (22)$$

Comparing variances (19) and (22) it follows that:

$$\sigma_{123}^2 < \sigma_{13}^2 \text{ for } 1 \leq z \leq 2 \text{ and } \forall \mu$$

$$\sigma_{123}^2 < \sigma_{13}^2 \text{ for } 0 \leq z < 1 \text{ and } \mu > -1 + \sqrt{\frac{z-2}{z-1}}.$$

When distance  $z > 1$ , the preferred path is the one along the sequence of transitions  $\mathbf{x}_1 \rightarrow \mathbf{x}_2 \rightarrow \mathbf{x}_3$  instead of  $\mathbf{x}_1 \rightarrow \mathbf{x}_3$  as this choice gives the *a posteriori* pdf with the smaller variance (and larger value). On the contrary, when the distance  $z < 1$ , the

choice depends on the ratio  $\mu = \sigma^2/\sigma_\phi^2$  in (20) that is related to the temporal resolution properties of the signature.

#### REFERENCES

- [1] D. A. Herron, "Horizon autopicking," *Leading Edge*, vol. 19, no. 5, pp. 491–492, 2000.
- [2] C. A. Woodham, W. A. Sandham, and T. S. Durrani, "3-D seismic tracking with probabilistic data association," *Geophys.*, vol. 60, no. 4, pp. 1088–1094, 1995.
- [3] K. Y. Huang, "Seismic horizon picking using a Hopfield network," in *Geophysical Applications of Artificial Neural Networks and Fuzzy Logic*. Norwell, MA: Kluwer, 2000.
- [4] I. Idier and Y. Goussard, "Multichannel seismic deconvolution," *IEEE Trans. Geosc. Remote Sensing*, vol. 31, pp. 961–979, Sept. 1993.
- [5] N. Bienati and U. Spagnolini, "Multidimensional wavefront estimation from differential delays," *IEEE Trans. Geosci. Remote Sensing*, vol. 39, pp. 655–664, Mar. 2001.
- [6] A. P. Pentland, "Fractal-based description of natural scenes," *IEEE Trans. Pattern Anal. Machine Intell.*, vol. PAMI-6, pp. 661–674, Nov. 1984.
- [7] M. Nicoli, V. Rampa, and U. Spagnolini, "Multitarget detection/tracking based on hidden Markov models," in *Proc. IEEE Int. Conf. on Acoustics, Speech, and Signal Processing—ICASSP 2000*, June 2000, pp. 3196–3199.
- [8] O. Lohlein and M. Fritzsche, "Classification of GPR data for mine detection based on hidden Markov models," in *Proc. IEE Conf. Detection of Abandoned Land Mines*, Oct. 1998, pp. 96–100.
- [9] Y. He and A. Kundu, "2-D shape classification using hidden Markov model," *IEEE Trans. Pattern Anal. Machine Intell.*, vol. 13, pp. 1172–1184, Nov. 1991.
- [10] R. L. Streit and R. F. Barret, "Frequency line tracking using hidden Markov models," *IEEE Trans. Acoust., Speech, Signal Processing*, vol. 38, pp. 586–598, Apr. 1990.
- [11] X. Xie and R. J. Evans, "Multiple target tracking and multiple frequency line tracking using hidden Markov models," *IEEE Trans. Signal Processing*, vol. 39, pp. 2659–2676, Dec. 1991.
- [12] U. Spagnolini and V. Rampa, "Multitarget detection/tracking for monostatic ground penetrating radar: Application to pavement profiling," *IEEE Trans. Geosci. Remote Sensing*, vol. 37, pp. 383–394, Jan. 1999.
- [13] O. Yilmaz, *Seismic Data Processing: Soc. Exploration Geophys.*, 1987.
- [14] Y. Bar-Shalom and X. R. Li, *Estimation and Tracking: Principles, Techniques, and Software*. Norwood, MA: Artech House, 1993.
- [15] L. R. Rabiner, "A tutorial on hidden Markov models and selected applications in speech recognition," *Proc. IEEE*, vol. 77, pp. 257–285, Feb. 1989.
- [16] G. D. Forney Jr, "The Viterbi algorithm," *Proc. IEEE*, vol. 61, pp. 268–277, Mar. 1973.
- [17] S. Fortune, "A sweepline algorithm for Voronoi diagram," *Algorithmica*, vol. 2, pp. 153–174, 1987.
- [18] E. Horowitz, S. Sahni, and S. Anderson-Freed, *Fundamentals of Data Structures in C*. Singapore: Computer Science, 1993.
- [19] F. Aminzadeh, N. Burkhard, P. Lailly, F. Rocca, and K. Wyatt, "Progress report from the SEG/EAEG 3-D modeling committee," *Leading Edge*, vol. 13, pp. 110–112, 1994.

**Monica Nicoli** (M'99) received the M.Sc. degree (cum laude) and Ph.D. degree in telecommunication engineering from Politecnico di Milano, Milan, Italy, in 1998 and 2002, respectively.

She spent March–August 2001 as a Visiting Researcher at the Signal and System Group, Department of Material Science, Uppsala University, Sweden. Currently, she is working at Dipartimento di Elettronica e Informazione, Politecnico di Milano, Italy. Her research interests include multitarget detection and tracking for remote sensing applications, and array signal processing for mobile communication systems.

**Vittorio Rampa** was born in Genoa, Italy, in 1957. He received the Laurea degree (with honors) in electronic engineering in 1984 from Politecnico di Milano, Milan, Italy.

He has been a Senior Researcher at the Center for Space Communication-National Research Council (CSTS-CNR), Milan, since 1986. He was a Visiting Scholar at the Center for Integrated Systems, Stanford University, Stanford, CA, from 1987 to 1988. His research interests include signal processing for radar and mobile communication systems.

**Umberto Spagnolini** (M'99), received the Dott. Ing. Elett. degree in telecommunications (cum laude) from Politecnico di Milano, Milan, Italy, in 1988.

Since 1988, he has been with the Dipartimento di Elettronica e Informazione, Politecnico di Milano, where he held the position of Associate Professor of digital signal processing since 1998. His primary research (and applications) focuses on array processing and wavefield interpolation (mobile communication and geophysics), inverse problems (ground penetrating radar), parameter estimation (2-D phase unwrapping for SAR), and non-Gaussian EMI reduction.

Dr. Spagnolini is a member of the SEG and EAGE and serves as an Associate Editor for the IEEE TRANSACTIONS ON GEOSCIENCE AND REMOTE SENSING. He was awarded the Associazione Elettronica Italiana (AEI) Award and the Van Weelden Award of EAGE, both in 1991, and received the Best Paper Award from EAGE in 1998.